Hydrothermal synthesis of $PrVO_4$ nanocubes with enhanced photocatalytic performance through a synergistic effect

Li Li ✉, *Zhimei Sun, Mai Xu, Jiewei Rong, Longde Wang, Yi Chen, Lujiang Wang, Fengwu Wang*

School of Chemistry and Materials Engineering, Huainan Normal University, Huainan 232038, People's Republic of China
✉ *E-mail: lli@mail.ustc.edu.cn*

Published in Micro & Nano Letters; Received on 22nd July 2019; Revised on 20th November 2019; Accepted on 4th December 2019

Novel tetragonal $PrVO_4$ nanocubes have been fabricated by a simple and green hydrothermal method. The excellent catalytic activity of the samples was investigated for the degradation of methylene blue aqueous solution under visible light irradiation. As compared with pure $PrVO_4$ and H_2O_2, the photocatalytic efficiency of the $PrVO_4/H_2O_2$ system was enhanced about 1.5 and 9 folds, respectively. In the whole photocatalytic process, h^+ and ·OH radicals played the dominant roles on the basis of the trapping test. The significantly enhanced photocatalytic activity was attributed to the synergistic effect between photocatalytic oxidation of $PrVO_4$ and heterogeneous photo-Fenton-like reaction of $V(V)/H_2O_2$. Finally, a possible photocatalytic mechanism was proposed.

1. Introduction: In modern society, environmental pollution and energy crisis have become more and more serious due to the industrialisation and globalisation. Photocatalytic technology has more advantages because of its applications in organic synthesis and the abatement of pollutants in water and air through harvesting solar energy [1–3]. Metal–oxide–semiconductor photocatalysts are attractive since they can eliminate organic contaminants efficiently without causing additional damage to the environment [4, 5]. In the heterogeneous photocatalysis field, titanium dioxide (TiO_2) is the most popular material with some prominent properties, but the relatively wide bandgap (3.2 eV) limits its visible (Vis) light harvest [6, 7].

Rare earth orthovanadates, as the cohesive class of materials easy for charge transfer [8], have potential applications in various fields. A variety of vanadates, such as $CeVO_4$, $LaVO_4$, $PrVO_4$, $GdVO_4$, YVO_4, $HoVO_4$, and $NdVO_4$ have been synthesised and examined as catalysts, photoluminescence, gas sensors, solar cells, optical fibres, and humidity sensors [9–12]. Owing to the generation of large amounts of hydroxyl radicals, advanced oxidation processes have shown great potential for degrading various organic pollutants from wastewater in the last decade [13–18]. Similar to the photo-Fenton-like reaction of ferrous salt, it is believed that the vanadate compounds can be activated by a small amount of H_2O_2 through the following three-step reaction [19, 20]:

$$\equiv V(V) + H_2O_2 \rightarrow \equiv V(IV) + H^+ + \cdot OOH$$

$$\equiv V(V) + \cdot OOH \rightarrow \equiv V(IV) + H^+ + O_2$$

$$\equiv V(IV) + H_2O_2 \rightarrow \equiv V(V) + OH^- + \cdot OH$$

Owing to the application of homogeneous Fenton's reagent is limited by the narrow working pH and the need for separation and recovery of the iron species [15], the heterogeneous Fenton-like reactions can eliminate pollutants efficiently relatively. Therefore, some other multivalent metal oxides, such as cobalt, manganese, cerium and copper oxides, have also been used as Fenton-like catalysts for the activation of H_2O_2 to overcome these drawbacks and extend the working pH range [17]. So, the development of new type and effective heterogeneous Fenton or photo-Fenton-like catalysts is a challenge [21–23].

In this Letter, we report that the well-crystallised tetragonal $PrVO_4$ nanocubes were controlled synthesis by a simple two-step hydrothermal method. The photocatalytic performances of $PrVO_4$ were evaluated by photodegrading organic dye methylene blue (MB) under 500 W Xenon lamp irradiation. To our best knowledge, $PrVO_4$ used as a photo-Fenton-like catalyst has not been investigated. A possible catalytic mechanism for the $PrVO_4/H_2O_2$ systems was proposed.

2. Experimental

2.1. Synthesis of $PrVO_4$ nanocubes: Sodium vanadate and praseodymium nitrate were supplied from Aladdin. The other reagents were purchased from Sinopharm. All reagents were of analytical grade and used without further purification. In the typical preparation of $Pr(OH)_3$ precursor, 2.227 g $Pr(NO_3)_3{\cdot}6H_2O$ and 1.602 g NaOH were dissolved into 20 ml ultrapure water to form a transparent solution, respectively. Then NaOH solution was added drop wise into $Pr(NO_3)_3{\cdot}6H_2O$ solution with vigorous stirring, and finally, the pH of the colloidal mixture was adjusted to around 14. The as-obtained emulsion was transferred into a Teflon-lined stainless steel autoclave after stirring for another 30 min and maintained at 140°C for 12 h. After centrifugation, the white $Pr(OH)_3$ nanorods were obtained. Nanocube-like $PrVO_4$ was synthesised by the hydrothermal conversion of $Pr(OH)_3$ precursor. Firstly, 5 mmol $Pr(OH)_3$ powders were suspended into 30 ml deionised water under ultrasonication for 60 min at ambient temperature and 15 mmol Na_3VO_4 was dissolved in 30 ml of ultrapure water. Then the Na_3VO_4 transparent solution was poured into the $Pr(OH)_3$ suspension drop wise with continuous stirring. A homogeneous mixture was obtained with a pH value of about 13 after stirring 1 h. Finally, the solution was transferred to a 100 mL Teflon-lined autoclave and heated at 180°C for 24 h and then was allowed to naturally cool down to room temperature. The faint pale yellow precipitate was separated, washed three times with distilled water and absolute alcohol, respectively, and finally centrifuged and dried in a vacuum oven at about 80°C overnight.

2.2. Characterisation of samples: The phase and crystal structure of $Pr(OH)_3$ and $PrVO_4$ samples were examined by the Bruker-AXS D8 powder X-ray diffraction (XRD) method using Cu K_α-radiation ($\lambda = 1.540598$ nm) operated 40 kV and 40 mA, respectively, and the diffractograms were recorded over the 2θ range 10–80°. The morphology of $PrVO_4$ and its precursor were observed by using a KYKY-EM3200 scanning electron microscope (SEM) with an accelerating voltage of 25 kV and a Hitachi Model H-800 transmission electron microscope (TEM) with accelerating voltage 200 kV. The Shimadzu 2450 ultraviolet (UV)–Vis

doi: 10.1049/mnl.2019.0455

spectrophotometer with a cuvette recorded the absorption curve of dye, and the absorption spectrum of the powder samples also was measured on it equipped with an integrating sphere attachment with $BaSO_4$ as a reflectance standard.

2.3. Photocatalytic degradation: The photochemical reaction apparatus (Zhengqiao, ZQ-GHX-V) was used to measure photocatalytic activities of $PrVO_4$ nanocubes. 15 mg of the sample was added into 15 ml aqueous solution of MB in the different cylindrical quartz vessel and kept in the reaction chamber for 1 h with stirring before illumination. After adsorption–desorption equilibrium was achieved, the photocatalytic process was initiated under a 500 W Xe-arc lamp irradiation equipped with 400 nm optical cut-off filters at ambient temperature (20°C) that was maintained through a fan and circulating water. At an interval of 20 min, 3 ml mixture of photocatalyst and dye was taken and centrifuged. The absorbance of MB was measured by monitoring the characteristic wavelength of 663 nm using the UV-Vis spectrophotometer.

3. Results and discussion: Fig. 1 exhibits the XRD patterns of the samples. The intensive diffraction peaks of $Pr(OH)_3$ are observed at $2\theta = 15.53°$, 27.51°, 28.40°, 39.97°, 50.95°, and 66.36°, which matched well with the (100), (110), (101), (201), (102), and (220) crystal planes of hexagonal $Pr(OH)_3$ (JCPDS Card No. 45-0086). For pure $PrVO_4$, there is a series of sharp and pointed diffraction peaks, which are in good consistent with the tetragonal phase of $PrVO_4$ (JCPDS Card No. 17-0341) with the lattice constants of $a = b = 7.358$ Å, $c = 6.462$ Å and a space group $I41/amd$ [141] without any impurity. The XRD patterns confirm that the phase-pure $PrVO_4$ powders were formed through the two-step hydrothermal conversion process.

The morphological features of $Pr(OH)_3$ and $PrVO_4$ were examined with SEM and TEM. Observed from the images as shown in Figs. 2*a* and *c*, the $Pr(OH)_3$ precursor exhibits well-defined 1D nanorods with a width of 10–30 nm and length of 60–100 nm. From Figs. 2*b* and *d*, it is evident that the pure orthorhombic polyhedron-like $PrVO_4$ was formed after the hydrothermal conversion for 24 h. The acquired samples have a uniform morphology feature and the mean particle size is ∼10–30 nm. At high temperature and pressure, the rod-like $Pr(OH)_3$ nanostructures gradually crystallised into smaller size nanoparticles, and finally completely converted to $PrVO_4$ nanocubes after the hydrothermal treatment.

X-ray photoelectron spectroscopy (XPS) can provide significant surface information and has been applied to characterise functional materials extensively. The survey XPS spectrum (Fig. 3) shows a small amount of C 1s peak located at 284.8 eV, resulting from adventitious hydrocarbons from the XPS instrument itself. It can be taken as the standard signal to calibrate other peaks [24].

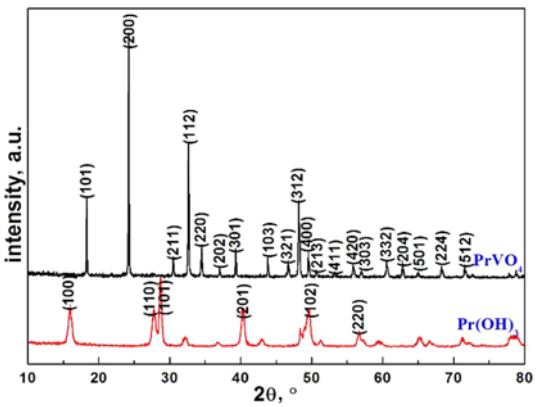

Fig. 1 *XRD patterns of $Pr(OH)_3$ and $PrVO_4$*

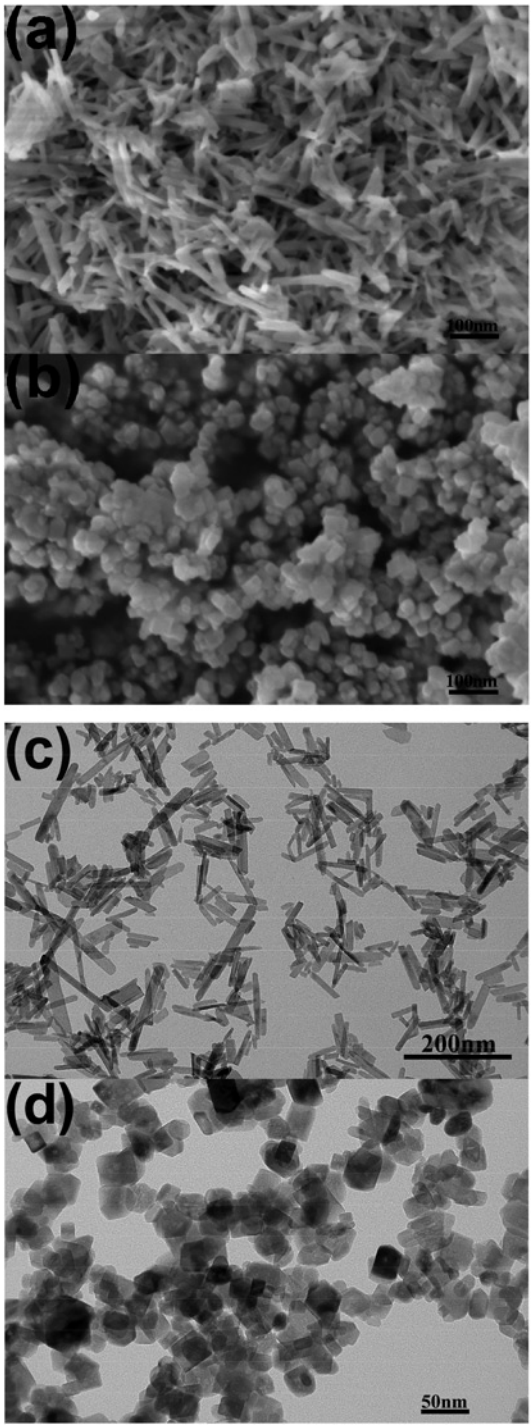

Fig. 2 *SEM and TEM images of precursor*
a, c $Pr(OH)_3$
b, d $PrVO_4$

No peaks of other elements could be found except C, Pr, V, and O, which indicates that the sample consists of praseodymium and vanadium composite oxide. The spectra agree well with the reported results in the literature [25]. In combination with the XRD, TEM and XPS results, it is confirmed that the as-prepared products are a tetragonal phase $PrVO_4$ nanocubes.

Fig. 4 shows the optical absorption spectrum of the as-obtained $PrVO_4$ sample from 200 to 800 nm. Owing to charge transitions from O 2p to Pr 4f orbits, we can observe the strong absorption edge of the sample at about 420 nm. The corresponding optical bandgap for the semiconductor can be deduced by drawing

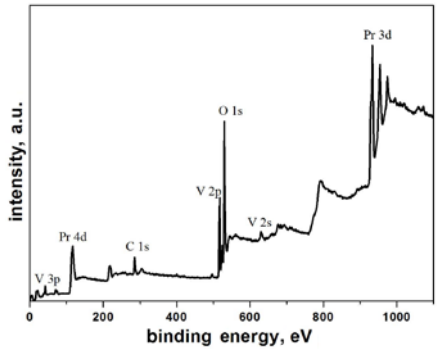

Fig. 3 *XPS survey spectra of $PrVO_4$ nanocubes*

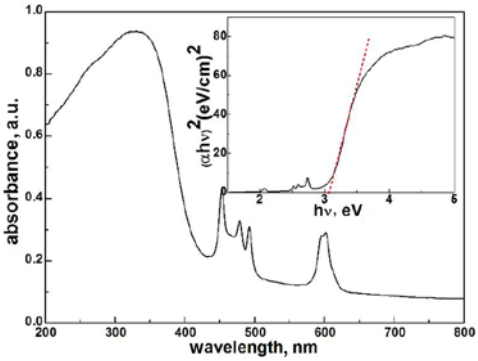

Fig. 4 *UV–vis diffuse reflectance spectrum of $PrVO_4$ photocatalyst (inset shows the estimated bandgap by the Kubelka–Munk function)*

tangent (the inset of Fig. 4) according to the following equation:

$$(\alpha h\nu)^n = B(h\nu - E_g)$$

where the electronic transition of the semiconductor defines the value of the index n. Owing to $PrVO_4$ as a direct bandgap material, the value of n is 2. α is the absorption coefficient and $h\nu$ is the incident photon energy. E_g is the bandgap energy obtained by extrapolating the straight portion of the $(\alpha h\nu)^2$ against the $h\nu$ plot to the point $\alpha = 0$. By the linear extrapolation, the bandgap of $PrVO_4$ was estimated at about 3.06 eV, which is slightly larger than the value reported in the literature [26, 27]. There are several absorption bands located in 329, 454, 478, 492 and 602 nm in the UV and Vis region of the sample. In $PrVO_4$ semiconductors, the valence band (VB) top is mainly composed of the 4f energy level of Pr and the conduction band (CB) bottom is mainly composed of the 2p energy level of O. The absorption spectrum can be explained by calculating the electron characteristics of $PrVO_4$ by density functional theory [28, 29]. The absorption peak of 329 nm (3.77 eV) may be the result of VO_4^{3-} electron transition, corresponding to the electron transition from the 2p non-bonding orbital of O to the 3d and 2p antibonding orbital of O [30, 31]. The absorption peaks of 454 nm (2.73 eV), 478 nm (2.59 eV), 492 nm (2.52 eV) and 602 nm (2.06 eV) were mainly caused by Pr^{3+} 4f electrons jumping from $^3H_4$ to $^2P_2$, $^3P_1$, $^3P_0$ and $^3H_6$ [32]. Therefore, the tetragonal zircon-type $PrVO_4$ polyhedron may be a photocatalytic material with a Vis light response.

MB was used as a model pollutant to evaluate the Vis light degradation activities of $PrVO_4$ nanopolyhedrons after physical adsorption in the dark. The concentrations of MB decreased by 20.3% and 55.4% in the $PrVO_4$ and $PrVO_4/H_2O_2$ system, respectively, after the adsorption–desorption equilibrium in the dark indicating that a Fenton-like reaction occurred in the $PrVO_4/H_2O_2$ system. Degradation efficiencies (De) were calculated according to the following formula:

$$\mathrm{De}(\%) = \frac{C}{C_0} \times 100\% = \frac{A}{A_0} \times 100\%$$

As shown in the $PrVO_4$/MB system (Fig. 5*a*), the highest degradation efficiency of 61.08% after 160 min irradiation was determined by the characteristic absorption peak of MB at 663 nm. When a small number of H_2O_2 was added into $PrVO_4$/MB suspension, the characteristic absorbance decreased quickly (Fig. 5*b*). From Fig. 5*c*, it can be seen that the degradation efficiencies reach above 51.87% and 87.03% after Vis-light illumination for 20 and 80 min, respectively. After the irradiation for 160 min, the degradation efficiency can reach 96%. The degradation of MB is greatly enhanced with the simultaneous presence of $PrVO_4$ and H_2O_2, suggesting that the addition of H_2O_2 can obviously accelerate the degradation of MB [33]. Hence, the roles of H_2O_2 in the $PrVO_4/H_2O_2$ photocatalytic system can be divided into two aspects: (i) to form ·OH radicals with the interfacial $^{\circ}V^{V}$ of $PrVO_4$ nanoparticles through Fenton-like reaction [34, 35] (1), (2), (ii) to trap the photogenerated electron forming ·OH radicals. Moreover, the *N*-demethylation of the dimethylamino group in MB molecule through oxidative degradation results in a hypsochromic shift and broadening of the absorption band with the increase of irradiation time. The hydroxylation/oxidation of MB

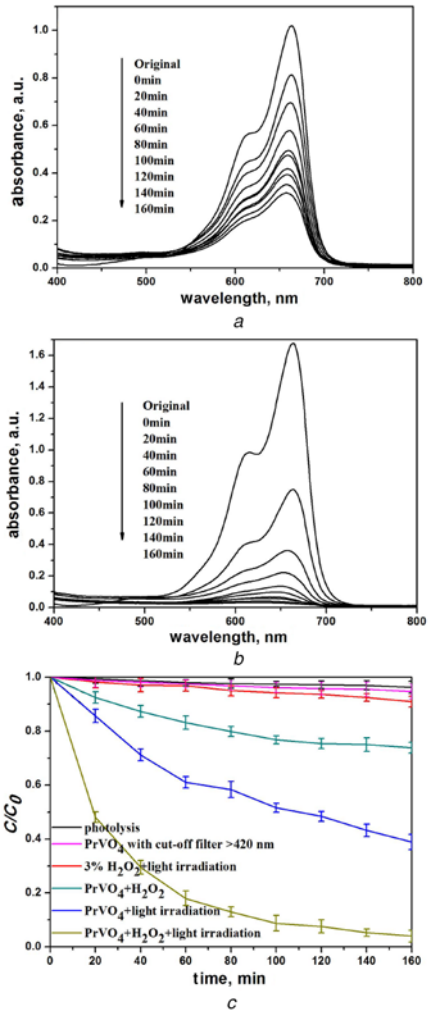

Fig. 5 *Evolutions of MB absorption spectra in the presence of*
a $PrVO_4$
b $PrVO_4 + H_2O_2$ with irradiation time
c Photodegradation efficiencies of MB as a function of irradiation time at different conditions

doi: 10.1049/mnl.2019.0455

is a predominant procedure, which is in good consistent with other literature [36, 37]. Based on the above discussion, nanoscaled $PrVO_4$ can catalyse the activation of H_2O_2 to produce OH radicals through Fenton-like reaction, the greatly enhanced photocatalytic behaviour $PrVO_4$–H_2O_2 system can be ascribed to the synergistic effect of heterogeneous Fenton-like reaction and semiconductor photocatalytic-oxidation [38].

To further investigate the photodegradation activity mainly dependent on the oxidative species over the $PrVO_4$–H_2O_2 system, the trapping experiment was performed. Benzoquinone (BQ), isopropyl alcohol (IPA), ethylenediamine tetra acetic acid disodium (EDTA-2Na), and potassium persulphate (PP) were added to the reaction solution as superoxide radical ($\cdot O_2^-$), hydroxyl radical ($\cdot OH$), photo-excited hole (h^+) and electron scavengers, respectively [39, 40]. From Fig. 6, the photocatalytic rate of the $PrVO_4$–H_2O_2 system was partially inhibited in the presence of all the scavengers except PP, which means that e^- is trapped completely by H_2O_2 during the photodegradation. On the other hand, the major role of holes can be identified by a significant decrease of photocatalytic performance in the presence of EDTA-2Na. Moreover, only 21 and 34% of MB can be removed when IPA and BQ were added within 160 min, respectively, indicating $\cdot OH$ and $\cdot O_2^-$ radicals as the predominant reactive oxygen species in the reaction system. It could be seen from the experimental results that h^+, $\cdot OH$ and $\cdot O_2^-$ radicals are the main active species in the $PrVO_4$–H_2O_2 photocatalytic process. The schematic illustration of the whole degradation mechanism of MB over $PrVO_4$ is illustrated in Fig. 7.

Based on the above experiments and analysis, we can elucidate the possible photocatalytic mechanism of the $PrVO_4$–H_2O_2 system. According to the classic Mulliken electronegativity theory, the VB and CB potentials of $PrVO_4$ semiconductor at the point of zero charge can be calculated by following empirical equation [41, 42]:

$$E_{CB} = \chi - E_e - 0.5E_g$$

$$E_{CB} = E_{VB} - E_g$$

where χ is the absolute electronegativity of the semiconductor. It is expressed as the geometric average of the Pearson absolute electronegativity of the constituent and can be calculated by the equation

$$\chi = \sqrt[N]{\chi_1^p \chi_2^m \cdots \chi_n^q}$$

(for $PrVO_4$, χ is 5.54 eV). E_e is the energy of free electrons on the hydrogen scale (4.5 eV), and E_{VB} and E_{CB} are the VB top and the CB bottom edge energy, respectively. The E_{VB} and E_{CB} of $PrVO_4$ can be determined as 2.57 and −0.49 eV (versus NHE). In terms of $PrVO_4$ photocatalyst, the CB potential (−0.49 eV) is more negative than the $O_2/\cdot O_2^-$ (−0.33 eV). So the electrons at CB (e_{CB}^-) can react with O_2 adsorbed on the surface of the catalyst to generate active $\cdot O_2^-$, which are an important oxidising species during MB degradation [43]. At the same time, the standard reduction potential $H_2O/\cdot OH$ (2.27 eV) is below the VB potential (2.57 eV) of $PrVO_4$, so the photogenerated holes in the VB of photocatalyst will react with H_2O to produce $\cdot OH$ radicals and further react with MB. Also, the VB holes can be directly involved in the photocatalytic degradation of organic contaminants.

On the basis of the above results, the degradation of MB can be increased greatly in the presence of small H_2O_2. It should be attributed to more $\cdot OH$ radicals generated by the synergistic effects of the photo-Fenton-like reaction between $PrVO_4$ and H_2O_2. The heterogeneous photo-Fenton-like catalytic mechanism is proposed as follows:

$$\equiv V^V + H_2O_2 + h\nu \rightarrow \equiv V^{IV} + \cdot OOH + H^+ \quad (1)$$

$$\equiv V^{IV} + H_2O_2 + h\nu \rightarrow \equiv V^V + \cdot OH + OH^- \quad (2)$$

$$PRVO_4 + h\nu \rightarrow PRVO_4(e^- + h^+) \quad (3)$$

$$e^- + H_2O_2 \rightarrow OH^- + \cdot OH \quad (4)$$

$$e^- + O_2 \rightarrow \cdot O_2^- \quad (5)$$

$$h^+ + H_2O \rightarrow \cdot OH + H^+ \quad (6)$$

$$MB + h^+(\cdot OH, \cdot O_2^-) \rightarrow CO_2 + H_2O \quad (7)$$

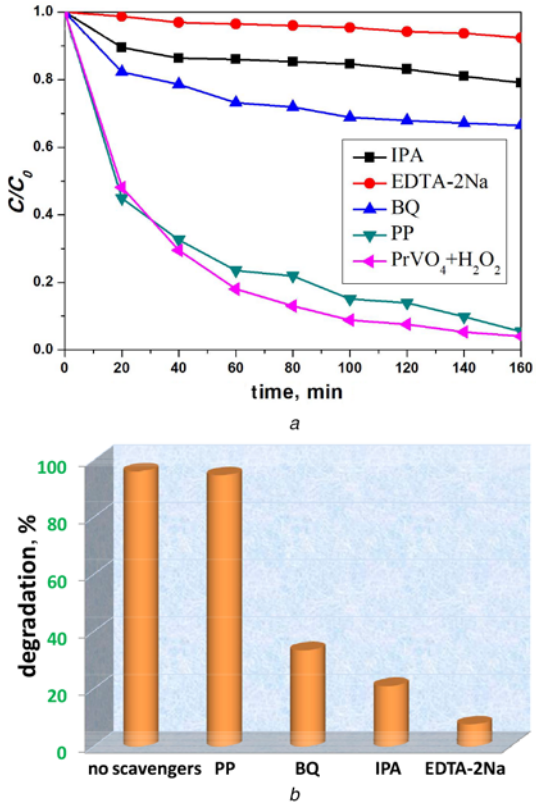

Fig. 6 *Effects of different scavengers on the degradation of MB over $PrVO_4$/H_2O_2 catalysts under visible light irradiation*
a Photodegradation of MB over the $PrVO_4/H_2O_2$ system in the presence of different scavengers
b The corresponding photodegradation efficiencies of MB illuminated for 160 min

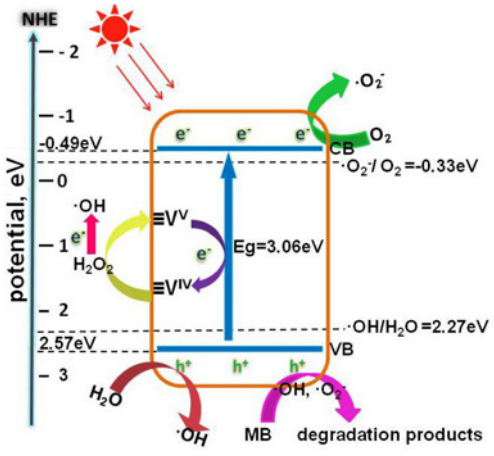

Fig. 7 *Schematic diagram of the photo-excited electron–hole separation process and the proposed mechanism for MB degradation*

4. Conclusion: Novel tetragonal $PrVO_4$ nanocubes were successfully prepared by a simple two-step hydrothermal method for the first time. The Vis-light-induced photocatalytic efficiency of $PrVO_4$ for MB degradation can reach 96% with the assistance of a small amount of H_2O_2 which is about 1.5- and 9-fold higher than that of $PrVO_4$ and H_2O_2 alone, respectively. The trapping experiments indicated that h^+ and ·OH played the dominant roles in the photocatalytic process. Furthermore, the synergistic effect mechanism was also elucidated based on the energy band positions and the photo-Fenton-like reaction of the resulting $PrVO_4$ nanostructures. These encouraging data demonstrate that the $PrVO_4$/H_2O_2 system has prospective application in the field of pollutants purification.

5. Acknowledgments: This work was supported by the Key Natural Science Foundation of Anhui Province (grant nos. KJ2015A160, KJ2015A208, and KJ2018A0465), the Key Excellent Young Talents Foundation of Anhui Province (grant no. gxyqZD2016262), the Key Science Foundation of Huainan Normal University (grant no. 2018xj15zd), and the Natural Science Foundation of Anhui Province (grant no. 1808085ME109).

6 References

[1] Li X.W., Xia J.X., Zhu W.S., *ET AL.*: 'Facile synthesis of few-layered MoS_2 modified BiOI with enhanced visible-light photocatalytic activity', *Colloids Surf. A, Physicochem. Eng. Aspects*, 2016, **511**, pp. 1–7

[2] Huang Y.K., Kang S.F., Yang Y., *ET AL.*: 'Facile synthesis of Bi/Bi_2WO_6 nanocomposite with enhanced photocatalytic activity under visible light', *Appl. Catal. B, Environ.*, 2016, **196**, pp. 89–99

[3] Ahmad R., Ahmad Z., Khan A.U., *ET AL.*: 'Photocatalytic systems as an advanced environmental remediation: recent developments, limitations and new avenues for applications', *J. Environ. Chem. Eng.*, 2016, **4**, pp. 4143–4164

[4] Zhu Z.F., Du J., Li J.Q., *ET AL.*: 'An EDTA-assisted hydrothermal synthesis of $BiVO_4$ hollow microspheres and their evolution into nanocages', *Ceram. Int.*, 2012, **38**, pp. 4827–4834

[5] Zhang Y.T., Liu C., Xu B.B., *ET AL.*: 'Degradation of benzotriazole by a novel Fenton-like reaction with mesoporous Cu/MnO_2: combination of adsorption and catalysis oxidation', *Appl. Catal. B, Environ.*, 2016, **199**, pp. 447–457

[6] Zhang L.Q., He X., Xu X.W., *ET AL.*: 'Highly active TiO_2/g-C_3N_4/G photocatalyst with extended spectral response towards selective reduction of nitrobenzene', *Appl. Catal. B, Environ.*, 2017, **203**, pp. 1–8

[7] Akhundi A., Yangjeh A.H.: 'Novel g-C_3N_4/Ag_2SO_4 nanocomposites: fast microwave-assisted preparation and enhanced photocatalytic performance towards degradation of organic pollutants under visible light', *J. Colloid. Interface. Sci.*, 2016, **482**, pp. 165–174

[8] Dolgos M.R., Paraskos A.M., Stolzfus M.W., *ET AL.*: 'The electronic structure of vanadate salts: cation substitution as a tool for band gap manipulation', *J. Solid State Chem.*, 2009, **182**, pp. 1964–1971

[9] He H.M., Zhang Y.J., Zhu W., *ET AL.*: 'Controlled synthesis, characterization, mechanism, and photoluminescence property of nanoerythrocyte-like $HoVO_4$ with high uniform size and morphology', *J. Cryst. Growth*, 2011, **329**, pp. 71–76

[10] Wang Y.B., Cao S.X., Shao M.J., *ET AL.*: 'Growth rate dependence of the $NdFeO_3$ single crystal grown by float-zone technique', *J. Cryst. Growth*, 2011, **318**, pp. 927–931

[11] Li T.T., Zhao L.H., He Y.M., *ET AL.*: 'Synthesis of g-C_3N_4/$SmVO_4$ composite photocatalyst with improved visible light photocatalytic activities in RhB degradation', *Appl. Catal. B, Environ.*, 2013, **129**, pp. 255–263

[12] Fan C.Y., Liu Q.Q., Ma T.D., *ET AL.*: 'Fabrication of 3D $CeVO_4$/graphene aerogels with efficient visible-light photocatalytic activity', *Ceram. Int.*, 2016, **42**, pp. 10487–10492

[13] Nie Y.L., Zhang L.L., Li Y.Y., *ET AL.*: 'Enhanced Fenton-like degradation of refractory organic compounds by surface complex formation of $LaFeO_3$ and H_2O_2', *J. Hazard. Mater.*, 2015, **294**, pp. 195–200

[14] Petrick A.S., Mauro B., Selene M.A., *ET AL.*: 'Enhancement of a solar photo-Fenton reaction with ferric–organic ligands for the treatment of acrylic-textile dyeing wastewater', *J. Environ. Manage.*, 2015, **152**, pp. 120–131

[15] Lan H.C., Wang A.M., Liu R.P., *ET AL.*: 'Heterogeneous photo-Fenton degradation of acid red B over Fe_2O_3 supported on activated carbon fiber', *J. Hazard. Mater.*, 2015, **285**, pp. 167–172

[16] Huang R., Fang Z., Yan X., *ET AL.*: 'Heterogeneous sono-Fenton catalytic degradation of bisphenol A by Fe_3O_4 magnetic nanoparticles under neutral condition', *Chem. Eng. J.*, 2012, **197**, pp. 242–249

[17] Wang Q., Ma Y., Xing S.T.: 'Comparative study of Cu-based bimetallic oxides for Fenton-like degradation of organic pollutants', *Chemosphere*, 2018, **203**, pp. 450–456

[18] Song J.M., Wang H., Hu G., *ET AL.*: '$ZnWO_4$–Cu system with enhanced photocatalytic activity by photo-Fenton-like synergistic reaction', *Mater. Res. Bull.*, 2012, **47**, pp. 3296–3300

[19] Kalal S., Chauhan N.P.S., Ameta N., *ET AL.*: 'Role of copper pyrovanadate as heterogeneous photo-Fenton like catalyst for the degradation of neutral red and azure-B: an eco-friendly approach', *Korean J. Chem. Eng.*, 2014, **31**, pp. 2183–2191

[20] Deng J.H., Jiang J.Y., Zhang Y.Y., *ET AL.*: '$FeVO_4$ as a highly active heterogeneous Fenton-like catalyst towards the degradation of Orange II', *Appl. Catal. B, Environ.*, 2008, **84**, pp. 468–473

[21] Soltanabadi Y., Jourshabani M., Shariatinia Z.: 'Synthesis of novel $CuO/LaFeO_3$ nanocomposite photocatalysts with superior Fenton-like and visible light photocatalytic activities for degradation of aqueous organic contaminants', *Sep. Purif. Technol.*, 2018, **31**, pp. 227–241

[22] Behzadifard Z., Shariatinia Z., Jourshabani M.: 'Novel visible light driven $CuO/SmFeO_3$ nanocomposite photocatalysts with enhanced photocatalytic activities for degradation of organic pollutants', *J. Mol. Liq.*, 2018, **15**, pp. 533–548

[23] Firak D.S., Orth E.S., Zamora P.P.: 'Unraveling the sigmoidal profiles in Fenton catalysis: toward mechanistic elucidation', *J. Catal.*, 2018, **361**, pp. 214–221

[24] Danish M., Gu X.G., Lu S.G.: 'An efficient catalytic degradation of trichloroethene in a percarbonate system catalyzed by ultra-fine heterogeneous zeolite supported zero valent iron–nickel bimetallic composite', *Appl. Phys. A, Gen.*, 2017, **531**, pp. 177–186

[25] Thirumalai J., Chandramohan R., Vijayan T.A., *ET AL.*: 'A novel 3D nanoarchitecture of $PrVO_4$ phosphor: selective synthesis, characterization, and luminescence behavior', *Mater. Chem. Phys.*, 2011, **127**, pp. 259–264

[26] Mahapatra S., Madras G., Guru T.N.R.: 'Synthesis, characterization and photocatalytic activity of lanthanide (Ce, Pr and Nd) orthovanadates', *Ind. Eng. Chem. Res.*, 2007, **46**, pp. 1013–1017

[27] Oshikiri M., Ye J.H., Boero M.: 'Inhomogeneous RVO_4 photocatalyst systems (R = Y, Ce, Pr, Nd, Sm, Eu, Gd, Tb, Dy, Ho, Er, Tm, Yb, Lu)', *J. Phys. Chem. C*, 2014, **16**, pp. 8331–8341

[28] Kresse G., Furtmuller J.: 'Semiconductors using a plane-wave basis set', *Comput. Mater. Sci.*, 1996, **6**, pp. 15–50

[29] Kresse G., Furtmuller J.: 'Efficient iterative schemes for ab initio total-energy calculations using a plane-wave basis set', *Phys. Rev. B*, 1996, **654**, pp. 11169–11186

[30] Dolgos M.R., Paraskos A.M., Stoltzfus M.W.: 'The electronic structures of vanadate salts: cation substitution as a tool for band gap manipulation', *J. Solid State Chem.*, 2006, **182**, pp. 1964–1971

[31] Ma J., Wu Q.S., Ding Y.P.: 'Selective synthesis of monoclinic and tetragonal phase $LaVO_4$ nanorods via oxides-hydrothermal route', *J. Nanopart. Res.*, 2008, **10**, pp. 775–786

[32] Benayas A., Jaque D., Hettrick S.J., *ET AL.*: 'Investigation of neodymium- diffused yttrium vanadate waveguides by confocal microluminescence', *J. Appl. Phys.*, 2008, **103**, pp. 1031041–1031046

[33] Luo W., Zhu L.H., Wang N., *ET AL.*: 'Efficient removal of organic pollutants with magnetic nanoscaled $BiFeO_3$ as a reusable heterogeneous Fenton-like catalyst', *Environ. Sci. Technol.*, 2010, **44**, pp. 1786–1791

[34] Kozlov Y.N., Romakh V.B., Kitaygorodskiy A., *ET AL.*: 'Oxidation of 2-propanol and cyclohexane by the reagent hydrogen peroxide-vanadate anion-pyrazine-2-carboxylic acid: kinetics and mechanism', *J. Phys. Chem. A*, 2007, **32**, pp. 7736–7752

[35] Nizova G.V., Kozlov Y.N., Shul'pin G.B.: 'Effect of acetonitrile on the catalytic decomposition of hydrogen peroxide by vanadium

doi: 10.1049/mnl.2019.0455

ions and conjugated oxidation of alkanes', *Russ. Chem. Bull.*, 2004, **10**, pp. 2330–2333
[36] Li L., Wang X., Zhang Y.G.: 'Enhanced visible light-responsive photocatalytic activity of $LnFeO_3$ (Ln = La, Sm) nanoparticles by synergistic catalysis', *Mater. Res. Bull.*, 2014, **50**, pp. 18–22
[37] Zhang T.Y., Oyama T., Aoshima A.: 'Photooxidative N-demethylation of methylene blue in aqueous TiO_2 dispersions under UV irradiation', *J. Photochem. Photobiol. A, Chem.*, 2001, **140**, pp. 163–172
[38] Li L., Wang X.: 'Self-propagating combustion synthesis and synergistic photocatalytic activity of $GdFeO_3$ nanoparticles', *J. Sol-Gel Sci. Technol.*, 2016, **79**, pp. 107–113
[39] He Y.M., Zhang L.H., Teng B.T.: 'New application of Z-scheme Ag_3PO_4/g-C_3N_4 composite in converting CO_2 to fuel', *Environ. Sci. Technol.*, 2015, **49**, pp. 649–656
[40] Ma L., Wang G.H., Jiang C.J.: 'Synthesis of core-shell TiO_2@g-C_3N_4 hollow microspheres for efficient photocatalytic degradation of rhodamine B under visible light', *Appl. Sur. Sci.*, 2017, **430**, pp. 263–272
[41] Zou L., Wang H.R., Yuan G.L.: 'Magnetically separable Cds/$ZnFe_2O_4$ composites with highly efficient photocatalytic activity and photostability under visible light', *ACS Appl. Nano Mater.*, 2018, **1**, pp. 831–838
[42] Luo J., Zhou X.S., Ning X.M.: 'Synthesis and characterization of Z-scheme In_2S_3/Ag_2CrO_4 composites with enhanced visible-light photocatalytic performance', *New J. Chem.*, 2017, **41**, pp. 845–856
[43] Xu D.F., Cheng B., Cao S.W.: 'Enhanced photocatalytic activity and stability of Z-scheme Ag_2CrO_4-GO composite photocatalysts for organic pollutant degradation', *Appl. Catal., B, Environ.*, 2015, **164**, pp. 380–388